Measurement of ^{134}Xe(n,2n)^{133m,g}Xe reaction cross sections in 14-MeV region with detailed uncertainty quantification

Jun-Hua Luo[1,2] · Jun-Cheng Liang[3] · Li Jiang[4] · Fei Tuo[5] · Liang Zhou[2] · Long He[1]

Abstract

A lead-shielded HPGe detector and offline γ-ray spectra of the residual product were used to measure the cross section (CS) and ratios of isomeric CS (σ_m/σ_g) in ^{134}Xe(n,2n)^{133m,g}Xe reactions at different energies (13.5 MeV, 13.8 MeV, 14.1 MeV, 14.4 MeV, 14.8 MeV) relative to the ^{93}Nb(n,2n)^{92m}Nb reaction CS. The target was high-purity natural Xe gas under high pressure. The T(d,n)^{4}He reaction produces neutrons. TALYS code (version 1.95) for nuclear reactions was used for calculations, with default parameters and nuclear level density models. The uncertainties in the measured CS data were thoroughly analyzed using the covariance analysis method. The results were compared with theoretical values, evaluation data, and previous experimental findings. CS data of the ^{134}Xe(n,2n)^{133m}Xe and ^{134}Xe(n,2n)^{133g}Xe reactions and the corresponding isomeric CS ratios at 13.5 MeV, 13.8 MeV, and 14.1 MeV neutron energies are reported for the first time. This research advances our knowledge of pre-equilibrium emission in the (n,2n) reaction channel by resolving inconsistencies in the Xe data.

Keywords ^{134}Xe(n,2n) reactions · 14-MeV neutrons · Cross sections (CSs) · Isomeric ratios (IRs) · Covariance analysis

1 Introduction

Reliable knowledge of neutron-induced cross sections (CSs) is required in nuclear power plants for energy and environmental protection, and in nuclear astrophysics reaction network calculations for vital input parameters [1–5]. Accurate measurements of CSs induced by neutrons at 14 MeV are desired for fusion reactors, nuclear transmutation, and nuclear model analyses [6–8]. Xe has nine stable isotopes [9]; 14-MeV neutrons can trigger nuclear reactions of Xe isotopes, including (n,α), (n,d), (n,p), (n,t), and (n,2n) [10, 11]. The ^{134}Xe(n,2n)^{133m,g}Xe CSs for such reactions were

experimentally obtained by two laboratories [12, 13] using sodium perxenate (Na$_4$XeO$_6$·2H$_2$O) and quinol clathrate targets, respectively. In general, preparation of this compound is complicated; the composition is complex, and it is difficult to ensure purity (Ref. (12) reported an Na$_4$XeO$_6$·2H$_2$O purity of 95.8%. Only one laboratory reported pure ground-state CSs in the ^{134}Xe(n,2n)^{133g}Xe reaction [12]. The excited-state, ground-state, total CS, and CS ratio for ^{134}Xe(n,2n)^{133m,g}Xe reactions correspond to a single energy value (14.4 MeV or 14.6 MeV). Extensive research on the excitation functions for ^{124,126,128,130,132,136}Xe(n,2n) and ^{130,131,132}Xe(n,p) reactions in the range of 13–15 MeV was recently reported by Bhatia et al. [14], Bhike et al. [15, 16], and Luo et al. [17, 18].

Our goal was to analyze four aspects of the ^{134}Xe(n,2n) reaction CS. First, the target ^{134}Xe isotope belongs to a transitional region ($N = 82$, below the closed neutron shell); an even ^{134}Xe nucleus for such shell closure is a good indicator of single-particle excitations [17]. Second, the half-life of the metastable state of the ^{133m,g}Xe pair is shorter than that of the ground state. This pair exhibits isomeric transition (IT) decay (Fig. 1). Third, published data on the ^{134}Xe(n,2n) reaction CS are scarce owing to difficulties in preparing gaseous targets for irradiation. Fourth, significant discrepancies

✉ Jun-Hua Luo
  luojh71@163.com

1   Institute of New Energy, Hexi University, Zhangye 734000, China

2   School of Physics and Electromechanical Engineering, Hexi University, Zhangye 734000, China

3   National Institute of Metrology, Beijing 100029, China

4   Institute of Nuclear Physics and Chemistry, China Academy of Engineering Physics, Mianyang 621900, China

5   China CDC, National Institute for Radiological Protection, Beijing 100088, China
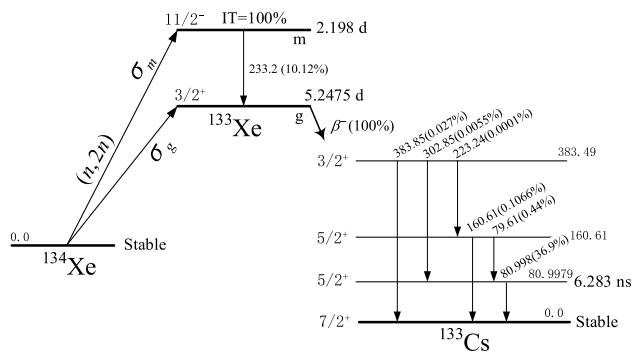
Fig. 1 Level schemes of isomeric pairs of ^{133m,g}Xe [9]. All energies are in keV

have been observed in published results [12, 13], mainly due to the following three factors:

i. Systematic inconsistencies are caused by differences in experimental techniques and conditions (neutron field characteristics, target sample, neutron monitoring method). Previous studies have used sodium perxenate ($Na_4XeO_6 \cdot 2H_2O$) and the solid quinol clathrate of Xe as the target materials [12, 13]. For neutron flux monitoring, Sigg and Kuroda (1976) [12] used a low-threshold reaction: ^{27}Al(n,α)^{24}Na (E_{th} = 3.25 MeV). Kondaiah et al. (1968) [13] used ^{136}Xe(n,2n)$^{135(m+g)}$Xe and ^{128}Xe(n,2n)$^{127(m+g)}$Xe reactions to monitor ^{134}Xe(n,2n)^{133m}Xe and ^{134}Xe(n,2n)$^{133(m+g)}$Xe nuclear reactions (Table 1).

ii. There is a significant shortage of decay data. The ^{134}Xe(n,2n)^{133m}Xe reaction CSs [12, 13] exhibited characteristic γ-ray intensities (14% and 13.55% at 233 keV, respectively (Table 1)). Recently, 10.12%

was also reported [9]. The ^{134}Xe(n,2n)^{133g}Xe reaction CSs were measured by Sigg and Kuroda (1976) [12], and Kondaiah et al. (1968) [13] using characteristic γ-ray intensities of 35% and 35.7%, respectively, for the same characteristic γ-ray of 81 keV (Table 1). However, 36.9% was obtained more recently [9]. As 79.61 keV and 80.998 keV γ-ray energies are so close that they cannot be distinguished by the detector, the intensity of the 81-keV gamma ray should be higher (37.34% = 0.44% + 36.9%). The CS of ^{133m}Xe radionuclide product with a 2.26-d half-life was also determined [12, 13], recently reported as 2.198 d [9].

iii. There are differences in the total CS measurement methods. Only two methods currently exist for calculating the total CS. (1) The excited-state and pure ground-state CSs can be added after measuring them separately [12]. (2) The ground state can be measured after full decay of the excited state via IT, and the result can be considered as the total CS [13]. The latter method satisfies the conditions that the excited-state half-life is less than that of the ground state, preferably much less, and IT = 100%. If these conditions are not satisfied, it is not advisable to replace the total CS with the obtained ground-state CS.

Analysis of the existing data led us to conclude that the isomeric ratios (IRs) and CSs for the (n,2n) reaction of ^{134}Xe in the 13–15 MeV range must be further analyzed. We used residual nuclear decay analysis [19–21] and natural Xe with high-purity pressure as the target to measure the ^{134}Xe(n,2n)^{133m}Xe, ^{134}Xe(n,2n)^{133g}Xe, and ^{134}Xe(n,2n)^{133}Xe CSs reactions and their corresponding isomeric-state CSs in the 13–15 MeV range. The results

Table 1 Literature indicating experimentally obtained CSs for ^{134}Xe(n,2n)^{133m,g}Xe reactions

Reaction	Decay data	Sample	Detector	Monitor reaction	E_n (MeV)	σ (mb)		Ref
^{134}Xe(n,2n)^{133m}Xe	$T_{1/2}$ = 2.26 d, $E\gamma$ = 232.8 keV, $I\gamma$ = 14%	$Na_4XeO_6 \cdot 2H_2O$	GeLi	^{27}Al(n,α)^{24}Na	14.6	655 ± 60	906 ± 83[a]	[12]
	$T_{1/2}$ = 2.26 d, $E\gamma$ = 233 keV, $I\gamma$ = 13.55%	Quinol clathrate	GeLi	^{136}Xe(n,2n)$^{135(m+g)}$Xe	14.4	665 ± 80	890 ± 107[a]	[13]
^{134}Xe(n,2n)^{133g}Xe	$T_{1/2}$ = 5.29 d, $E\gamma$ = 81.0 keV, $I\gamma$ = 35%	$Na_4XeO_6 \cdot 2H_2O$	GeLi	^{27}Al(n,α)^{24}Na	14.6 14.4	805 ± 90 1695 ± 226[b]	755 ± 84[a] 1366 ± 202[b]	[12] [13]
^{134}Xe(n,2n)$^{133(m+g)}$Xe	$T_{1/2}$ = 5.29 d, $E\gamma$ = 81.0 keV, $I\gamma$ = 35%	$Na_4XeO_6 \cdot 2H_2O$	GeLi	^{27}Al(n,α)^{24}Na	14.6	1460 ± 110	1661 ± 118[a]	[12]
	$T_{1/2}$ = 5.27 d, $E\gamma$ = 81 keV, $I\gamma$ = 35.7%	Quinol clathrate	GeLi	^{128}Xe(n,2n)$^{127(m+g)}$Xe	14.4	2360 ± 240	2256 ± 229[a]	[13]

a: corrected results using characteristic γ-ray intensity

b: Reference 13 does not provide ground-state CS values. This value was obtained by subtracting the excited-state CS value from the total CS value

were compared with theoretical values obtained using TALYS-1.95 [22], evaluation data, and previous experimental results.

2 Experimental Methods

2.1 Sample preparation

Naturally pure Xe (99.999%, 2.3–5.2 g) pressurized to 120–250 atm was placed in a 1-mm thick spherical stainless steel container 20 mm in diameter. The samples and monitors (niobium foil: $\Phi = 20$ mm, 0.12-mm thick, 99.99% pure; aluminum foil: $\Phi = 20$ mm, 0.3-mm thick, 99.999% pure), and zirconium foil ($\Phi = 20$ mm, 0.2-mm thick, 99.95% pure) were combined as ZrNbAl-Xe-AlNbZr for irradiation. The samples were mounted at different angles (0º, 45º, 90º, 110º, 135º) to the incident beam. The neutron-producing target edge was 5 cm from the sample center. Due to its high threshold energy, the ^{93}Nb(n,2n)^{92m}Nb (threshold energy 8.972 MeV) reaction was used to monitor the corresponding threshold energies of ^{134}Xe(n,2n)^{133m,g}Xe reactions ($E_{th} = 8.853$ MeV and 8.618 MeV). Low-threshold reactions such as (n,α) and (n,p) were monitored via a ^{27}Al(n,α)^{24}Na reaction (threshold energy = 3.249 MeV). The CS of the ^{93}Nb(n,2n)^{92m}Nb reaction was obtained from the IRDFF-II data library [23]. To minimize the influence of the ^{132}Xe(n,γ)^{133m,g}Xe reaction on the ^{134}Xe(n,2n)^{133m,g}Xe reaction, the samples were covered with Cd foil (1-mm thick, 99.95% pure). The details of this approach are presented in our previous studies [17, 18].

The neutron generator facility was provided by the China Academy of Engineering Physics (CAEP) for sample irradiation at $(4–5) \times 10^{10}$ n/s yield (for 2 h). The $d + {}^3H \rightarrow n + {}^4He + 17.6$ MeV reaction provided neutrons at 14 MeV with deuteron beam current and energy of 200 μA and 134 keV, respectively. The tritium–titanium target thickness was 2.65 mg/cm^2. A beam of α-particles at 135° was used to correct the neutron flux.

2.2 Neutron energy and detection efficiency

In the experiment, Zr and Nb were used to measure the CS ratios of ^{93}Nb(n,2n)^{92m}Nb and ^{90}Zr(n,2n)$^{89(m+g)}$Zr, respectively, to determine the neutron energy. At irradiation angles of 135°, 110°, 90°, 45°, and 0°, the energies were 13.5 MeV, 13.8 MeV, 14.1 MeV, 14.4 MeV, and 14.8 MeV, respectively. For verification purposes, the neutron energies were determined using different methods [24]. Considering the sample distance from the target, size, and beam radius, the uncertainty in the neutron energy was 0.2 MeV [25]. The results obtained using the CS ratio method were consistent in terms of the experimental errors. The detector efficiency was calibrated

using ^{152}Eu, ^{133}Ba, ^{137}Cs, and ^{226}Ra standard sources. The Monte Carlo method was used to adjust the data for the geometrical differences between the calibration sources applied to the HPGe detector and the Xe sphere efficiency determination. The details are provided in our previous studies [17, 18].

2.3 Radioactivity measurement

Five samples (No.1–5) were allowed to decay after irradiation for 2.9 d, 3.9 d, 5.0 d, 4.0 d, and 5.0 d, respectively. The γ-ray activities of ^{133m}Xe, ^{133g}Xe, and ^{92m}Nb nuclei were measured with a coaxial HPGe detector, with crystal diameter, length, relative efficiencies, and energy resolution (1.332 MeV) of 70.1 mm, 72.3 mm, 68%, and 1.69 keV, respectively. Typical γ-ray spectra obtained after 2.9 d of irradiation are shown in Fig. 2. A γ-spectrum analysis was performed using ORTEC® GammaVision® software to estimate the peak area [26].

Table 2 displays the natural isotope abundance and product decay characteristics.

3 CS calculations and associated uncertainties

3.1 CS calculation

The reaction CSs can be expressed as [17, 18]

$$\sigma_x = \frac{[S\varepsilon I_\gamma \eta KMD]_{Nb}}{[S\varepsilon I_\gamma \eta KMD]_x} \frac{[\lambda AFC]_x}{[\lambda AFC]_{Nb}} \sigma_{Nb} \qquad (1)$$

where Nb and x are the monitored and measured values, respectively; ε is the full-energy peak efficiency; I_γ represents the gamma-ray intensity; η is the abundance of the target nuclide; M is the mass of the sample;
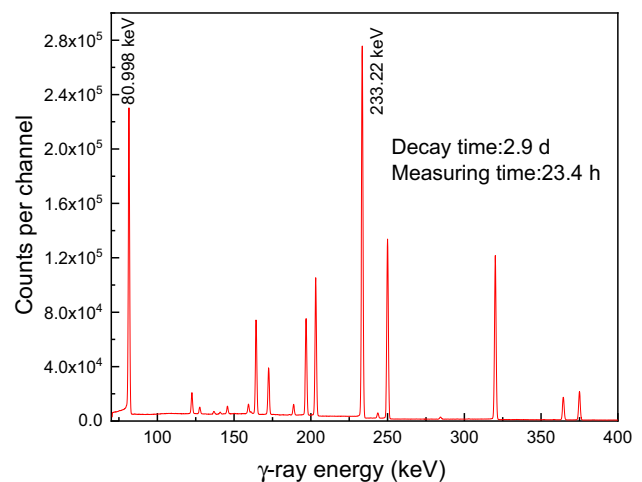
Fig. 2 Xe γ-ray spectrum after 2.9 d of decay after irradiation. Data were collected for 23.4 h

Table 2 Details of current ^{134}Xe(n,2n) nuclear reaction CS measurements (taken from ENSDF (2022) [9])

Isotope abundance (%)	Reaction	E-threshold (MeV)	Mode decay (%)	Product half-life	Eγ (keV)	Iγ (%)
10.4357_{21}	^{134}Xe(n,2n)^{133m}Xe	8.853	IT(100)	2.198 d$_{13}$	233.22	10.12_{15}
10.4357_{21}	^{134}Xe(n,2n)^{133g}Xe	8.618	β$^-$(100)	5.2475 d$_5$	80.998, 79.61	$36.9_3, 0.44_{18}$
100	^{93}Nb(n,2n)^{92m}Nb	8.972	EC (100)	10.15 d$_2$	934.44	99.15_4

Uncertainties are indicated by the lower index and italicized numbers 10.4357_{21}% indicates (10.4357 ± 0.0021)%, 2.198 d$_{13}$ indicates (2.198 ± 0.013) d

$D = e^{-\lambda t_1} - e^{-\lambda(t_1+t_2)}$ represents the counting collection factor; $S = 1 - e^{-\lambda T}$ is the growth factor of the product nuclide; T denotes the irradiation time; t_1 is the cooling time; t_2 is the measurement time; A is the atomic weight; C represents the measured full-energy peak area; λ is the decay constant of the residual nucleus; K is the correction factor for decaying nuclei during irradiation time (T), which is divided into small time intervals Δt_i. This factor is calculated as $K = \left[\sum_{i=1}^{n} \phi_i(1 - e^{-\lambda \Delta t_i})e^{-\lambda T_i}\right] / (S\phi)$, where ϕ_i is the mean neutron fluence rate of the ith part, and is regarded as a constant (when n is sufficiently large). T_i is the time from the end of the ith part to the end of total irradiation; $\phi = \sum_{i=1}^{n} \phi_i \Delta t_i / T$ is the mean neutron fluence rate within the irradiation time. F is the total correction factor, expressed as.

$$F = F_\Omega \times F_s \times F_g \tag{2}$$

where F_Ω, F_s, and F_g are the correction factors for the solid angle of the neutron flux, self-absorption of the specific γ-ray energy, and sample-counting geometry, respectively. F_s, F_g, and F_Ω were estimated using the characteristics of spherical samples, as described in Sect. 3.1 of Ref. [18]. Table 3 presents the self-absorption correction factors.

To obtain the pure ground-state CSs for ^{134}Xe(n,2n)^{133g}Xe reactions, C_x in Eq. (1) was set to a peak area of 80.998 keV minus the contribution from ^{133m}Xe via ^{133m}Xe $\xrightarrow{\text{IT(100\%)}}$ ^{133g}Xe (counting C_1). C_1 can be expressed using the decay of an artificial nuclide, expressed as [18]

$$C_1 = \frac{P_{mg}\varepsilon_g I_g C_m F_m(\lambda_g^2 S_m D_m - \lambda_m^2 S_g D_g)}{(\lambda_g - \lambda_m)S_m D_m I_m \varepsilon_m \lambda_g K_m F_g}, \tag{3}$$

where subscripts g and m are the ground and metastable states, respectively; P_{mg} is the percentage of metastable-state disintegrations that produce ground-state nuclides; C_m is the energy peak area of the metastable state; $S_m = 1 - e^{-\lambda_m T}$ and $S_g = 1 - e^{-\lambda_g T}$; I_m and I_g are the intensities of γ-rays, where ε_m and ε_g are the full-energy peak efficiencies of the metastable and ground states, respectively; K_m is the neutron-injection fluctuation indicator of the metastable state; F_m and F_g denote the correction factors of the metastable and ground states, respectively; D_m and D_g are coefficients defined as $D_m = e^{-\lambda_m t_1} - e^{-\lambda_m(t_1+t_2)}$ and $D_g = e^{-\lambda_g t_1} - e^{-\lambda_g(t_1+t_2)}$.

3.2 Associated experimental uncertainties

When calculating the main uncertainties of CS determination, we assumed that only the half-life uncertainty contributed to the uncertainty in the timing factor. The following parameters were used for this purpose: $C_{x,Nb}$ as the γ-ray

Table 3 Correction variables for sample self-absorption at different γ-ray energies

Gamma-ray energy (keV)	μ/ρ (cm^2/g)		μ (cm^{-1})			Sample density ρ (g/cm^3)	Correction factor f_s
	Fe	Xe	Fe	No	Xe		
80.998	0.584	3.5521	4.5906	1	4.4117	1.2420	8.288
				2	2.0804	0.5857	4.103
				3	4.2326	1.1916	7.956
				4	1.9529	0.5498	3.889
				5	1.9369	0.5453	3.863
233.22	0.134	0.3108	1.0533	1	0.386	1.242	1.39
				2	0.182	0.5857	1.204
				3	0.3703	1.1916	1.375
				4	0.1709	0.5498	1.195
				5	0.1695	0.5453	1.194

counting statistics, $M_{x,\text{Nb}}$ as the target masses, $I_{x,\text{Nb}}$ as the relative γ-ray intensities, η_x as the target isotopic abundance, σ_{Nb} as the standard CS, $\varepsilon_{x,\text{Nb}}$ as the efficiencies, and $S_{x,\text{Nb}}$ and $D_{x,\text{Nb}}$ as timing factors. The subscripts Nb and x correspond to the monitored and measured reaction-related terms, respectively.

For generative nuclei ^{133m}Xe and ^{133g}Xe, the uncertainty of correction factor F is estimated as 2.0% and 3.0%, respectively. These uncertainties were applied to assess the total uncertainty of the experimental CSs [27–30]. Tables 4 and 5 highlight the uncertainties in the

parameters contributing to the reaction CS values, which were used to extend the covariance matrix between different energy levels. All samples were investigated using the same setup and standard CS reaction. Thus, the detector efficiency and standard CS accuracy were consistent for all neutron energy correlations. After calculation of fractional uncertainties, covariance analysis calculated the correlation coefficients between each energy-related property. The coefficients and corresponding energies are presented in Table 6. The CS covariance matrix and total uncertainty were generated for energy-level pairs (e.g., $(\sigma_{xi},\sigma_{xj})$) using

Table 4 Uncertainties (%) in parameters for ^{134}Xe(n,2n)^{133m}Xe reaction CSs at 13.5–14.8 MeV

Attributes (x)	Fractional uncertainties (%)				
	13.5 MeV (Δx_i)	13.8 MeV (Δx_j)	14.1 MeV (Δx_k)	14.4 MeV (Δx_l)	14.8 MeV (Δx_n)
C_x	0.1236	0.1471	0.1349	0.1750	0.0726
C_{Nb}	0.8523	0.8102	0.8083	0.8164	0.9315
I_x	1.4822	1.4822	1.4822	1.4822	1.4822
I_{Nb}	0.0403	0.0403	0.0403	0.0403	0.0403
M_x	0.0401	0.0869	0.0816	0.0876	0.0385
M_{Nb}	0.0111	0.0109	0.0112	0.0110	0.0112
η_x	0.0201	0.0201	0.0201	0.0201	0.0201
σ_{Nb}	0.6327	0.5615	0.5461	0.5427	0.5645
ε_x	2.7201	2.7201	2.7201	2.7201	2.7201
ε_{Nb}	2.5038	2.5038	2.5038	2.5038	2.5038
S_x	0.5836	0.5836	0.5836	0.5836	0.5836
S_{Nb}	0.1965	0.1965	0.1965	0.1965	0.1965
D_x	0.4188	0.4197	0.2302	0.2335	0.0419
D_{Nb}	0.1857	0.1857	0.1858	0.1858	0.1860
F_x	2.0000	2.0000	2.0000	2.0000	2.0000
Total error (%)	4.65	4.63	4.62	4.62	4.63

Table 5 Uncertainties (%) in parameters for ^{134}Xe(n,2n)^{133g}Xe reaction CSs at 13.5–14.8 MeV

Attributes (x)	Fractional uncertainties (%)				
	13.5 MeV (Δx_i)	13.8 MeV (Δx_j)	14.1 MeV (Δx_k)	14.4 MeV (Δx_l)	14.8 MeV (Δx_n)
C_x	0.1198	0.1224	0.1115	0.1174	0.0936
C_{Nb}	0.8523	0.8102	0.8083	0.8164	0.9315
I_x	1.2854	1.2854	1.2854	1.2854	1.2854
I_{Nb}	0.0403	0.0403	0.0403	0.0403	0.0403
M_x	0.0201	0.0869	0.0816	0.0876	0.0385
M_{Nb}	0.0111	0.0109	0.0112	0.0110	0.0112
η_x	0.0201	0.0201	0.0201	0.0201	0.0201
σ_{Nb}	0.6327	0.5615	0.5461	0.5427	0.5645
ε_x	3.9743	3.9743	3.9743	3.9743	3.9743
ε_{Nb}	2.5038	2.5038	2.5038	2.5038	2.5038
S_x	0.0094	0.0094	0.0094	0.0094	0.0094
S_{Nb}	0.1965	0.1965	0.1965	0.1965	0.1965
D_x	0.0027	0.0039	0.0039	0.0039	0.0052
D_{Nb}	0.1857	0.1857	0.1858	0.1858	0.1860
F_x	3.0000	3.0000	3.0000	3.0000	3.0000
Total error (%)	5.83	5.82	5.82	5.82	5.83

the data from Tables 4–6 by adding 15 subset matrices in Eq. 4[29]:

$$\mathrm{Cov}(\sigma_{xi}, \sigma_{xj}) = \sum_i \sum_j \Delta x_i \times \mathrm{Cor}(\Delta x_i, \Delta x_j) \times \Delta x_j. \tag{4}$$

The generated covariance matrix was [5×5]. The uncertainty in the experimental CS value was determined as (Eq. 5) [29]

$$\mathrm{Cov}(\sigma_{xi}, \sigma_{xi}) = (\Delta\sigma_{xi})^2. \tag{5}$$

From the covariance matrix and total uncertainty between neutron energies, the correlation matrix [5×5] was derived using Eq. 6 [29]:

$$\mathrm{Cor}(\sigma_{xi}, \sigma_{xj}) = \frac{\mathrm{Cov}(\sigma_{xi}, \sigma_{xj})}{(\Delta\sigma_{xi}) \cdot (\Delta\sigma_{xj})}. \tag{6}$$

The experimentally obtained reaction CS values and their correlation matrices and uncertainties are presented in Tables 7 and 8.

Table 9 shows experimental values for $^{134}\mathrm{Xe}(n,2n)^{133(m+g)}\mathrm{Xe}$ reaction CSs and their IRs, and the monitor reaction CSs at different neutron energies.

Table 6 Correlation coefficients of parameters at 13.5–14.8 MeV for $^{134}\mathrm{Xe}(n,2n)^{133m,g}\mathrm{Xe}$ reaction CS. The I_x, I_{Nb}, η_x, σ_{Nb}, ε_{Nb}, S_{Nb}, and D_{Nb} subsets are fully correlated at these energies

Cor(Δx, Δx)	Correlation coefficient (Δx, Δx)							
	C_x	C_{Nb}	M_x	M_{Nb}	ε_x	S_x	D_x	F_x
(Δx_i, Δx_i)	1	1	1	1	1	1	1	1
(Δx_i, Δx_j)	0	0	0	0	0.9987	0	0	0
(Δx_i, Δx_k)	0	0	0	0	0.9987	0	0	0
(Δx_i, Δx_l)	0	0	0	0	0.9987	0	0	0
(Δx_i, Δx_n)	0	0	0	0	0.9987	0	0	0
(Δx_j, Δx_j)	1	1	1	1	1	1	1	1
(Δx_j, Δx_k)	0	0	0	0	0.9987	0	0	0
(Δx_j, Δx_l)	0	0	0	0	0.9987	0	0	0
(Δx_j, Δx_n)	0	0	0	0	0.9987	0	0	0
(Δx_k, Δ_k)	1	1	1	1	1	1	1	1
(Δx_k, Δx_l)	0	0	0	0	0.9987	0	0	0
(Δx_k, Δx_n)	0	0	0	0	0.9987	0	0	0
(Δx_l, Δx_l)	1	1	1	1	1	1	1	1
(Δx_l, Δx_n)	0	0	0	0	0.9987	0	0	0
(Δx_n, Δx_n)	1	1	1	1	1	1	1	1

Table 7 Experimental CSs (mb) of $^{134}\mathrm{Xe}(n,2n)^{133m}\mathrm{Xe}$ reaction and their overall uncertainties and correlation matrices

Neutron energy E_n (MeV)	Cross section σ_x (mb)	$\Delta\sigma_x$ (%)	Correlation matrix				
13.5±0.2	884±41	4.65	1.0000				
13.8±0.2	888±41	4.63	0.7565	1.0000			
14.1±0.2	909±42	4.62	0.7586	0.7593	1.0000		
14.4±0.2	916±42	4.62	0.7581	0.7588	0.7610	1.0000	
14.8±0.2	928±43	4.63	0.7562	0.7569	0.7591	0.7586	1.0000

Table 8 Experimental CSs (mb) of $^{134}\mathrm{Xe}(n,2n)^{133g}\mathrm{Xe}$ reaction and their overall uncertainties and correlation matrices

Neutron energy E_n (MeV)	Cross section σ_x (mb)	$\Delta\sigma_x$ (%)	Correlation matrix				
13.5±0.2	824±48	5.83	1.0000				
13.8±0.2	810±47	5.82	0.7125	1.0000			
14.1±0.2	786±46	5.82	0.7125	0.7129	1.0000		
14.4±0.2	767±45	5.82	0.7123	0.7127	0.7127	1.0000	
14.8±0.2	747±44	5.83	0.7105	0.7108	0.7108	0.7106	1.0000

Table 9 Experimental CSs (mb) of ^{134}Xe(n,2n)$^{133(m+g)}$Xe reaction and their IRs

E_n (MeV)	This study		Monitor reaction ^{93}Nb(n,2n)^{92m}Nb	
	CS (mb)	IRs (σ_m/σ_g)	CS (mb)	Reference
13.5 ± 0.2	1708 ± 63	1.07 ± 0.08	453.0 ± 2.9	[24]
13.8 ± 0.2	1698 ± 63	1.10 ± 0.08	457.4 ± 2.6	[24]
14.1 ± 0.2	1696 ± 62	1.16 ± 0.09	459.7 ± 2.5	[24]
14.4 ± 0.2	1683 ± 62	1.20 ± 0.09	460.1 ± 2.5	[24]
14.8 ± 0.2	1675 ± 61	1.24 ± 0.09	460.2 ± 2.6	[24]

4 Theoretical calculations

TALYS software is widely used to analyze pre-equilibrium mechanisms, direct nuclear reactions, and compound nuclei (CN). It can evaluate nuclear reactions in the range of 0.001–200 MeV for target nuclei with masses of 12 and higher. TALYS also calculates the nuclear reaction CSs. Theoretical calculations for different ratios of ^{134}Xe(n,2n)^{133m,g}Xe reactions (σ_m/σ_g) were performed for different ranges of neutron energies using TALYS-1.95 (ver. 1.95) [22]. We used the default parameters for our calculations, except for six distinct nuclear level density models (NLDs), which were divided into two groups: three microscopic levels and three phenomenological densities. The phenomenological level densities included: (1) ldmodel 1, with a constant temperature and Fermi gas model, and excitation energy divided into higher and lower energy regions in the Fermi gas model and with constant temperature laws, respectively; (2) ldmodel 2 is based on the back-shifted Fermi gas model, which uses the Fermi gas expression across the region; (3) ldmodel 3 is a generalized superfluid model that considers superconductive correlations based on Barden–Cooper–Schrieffer theory [31, 32]. The microscopic level densities are (i) ldmodel 4 is made up of Goriely's tables derived from the Skyrme force (microscopic level densities) [33]; (ii) ldmodel 5 consists of Hilaire's combinatorial tables derived from the Skyrme force [33]; (iii) ldmodel 6 is the Gogny force, derived from Hilaire's combinatorial tables [33]. Examining the spin distribution is feasible using relative feeding as a 'probe'. $\sigma_F^2(E_x)$ indicates the angular momentum distribution of the level density, expressed as:

$$\sigma_F^2(E_x) = 0.01389 \frac{A^{5/3}}{\tilde{a}} \sqrt{\alpha(E_x - \Delta)}, \tag{7}$$

where A indicates the mass number; E_x is the true excitation energy, Δ represents the empirical parameter and energy shift, which are nearly equal to the pairing energy of the observed nucleus odd–even effects; α is the energy-dependent level density parameter accounting for damping at higher excitation energies and shell effects at lower energies. Without shell effects, the asymptotic level density parameter ($\tilde{a}$) is equal to α [34].

5 Results and discussion

Tables 7, 8 and 9 show the CSs of the ^{134}Xe(n,2n)^{133m}Xe, ^{134}Xe(n,2n)^{133g}Xe, and ^{134}Xe(n,2n)^{133}Xe reactions and the corresponding isomeric-state CS ratios obtained using the activation method. The data of the excited state and pure ground state were compared to data from the literature [12, 13] and data obtained by TALYS-1.95 at six energy-level densities [22]. The ^{134}Xe(n,2n)^{133}Xe CS was also compared to data from the ENDF/B-VIII.0 [35], JEFF-3.3 [36], JENDL-4.0 [37], ROSFOND [38], and CENDL-3 [39] databases.

5.1 ^{134}Xe(n,2n)^{133m}Xe reaction

Two studies [12, 13] have reported ^{134}Xe(n,2n) experiments for the ^{133m}Xe reaction. However, they provide the CS at only one energy value (14.4 MeV or 14.6 MeV). For a γ-ray with 233.22 keV energy, Sigg and Kuroda [12] used $I_\gamma = 14\%$, and Kondaiah et al. [13] used $I_\gamma = 13.6\%$. However, other studies indicate that data measurement accuracy was higher with $I_\gamma = 10.12\%$. In this study, γ-ray energy of 233.22 keV with an intensity of $I_\gamma = 10.12\%$ emitted during the decay of ^{133m}Xe was used to obtain the ^{134}Xe(n,2n)^{133m}Xe reaction CS. Thus, the CS values were modified according to the following equation:

$$\sigma_{\text{corrected}} = \frac{I_{\gamma(\text{old})}}{I_{\gamma(\text{new})}} \sigma_{\text{literature}}, \tag{8}$$

where $\sigma_{\text{literature}}$ is the CS from the literature; $I_{\gamma(\text{old})}$ is the γ-ray intensity at 233.22 keV, and $I_{\gamma(\text{new})}$ is 10.12%. The experimental data are strongly correlated with the corrected experimental results [12, 13], as shown in Fig. 3. However, the data are below the TALYS-1.95 excitation curves (ldmodels 1–6) for neutrons with energies of 13.8–14.8 MeV. These findings were first published at 13.5-MeV, 13.8-MeV, and 14.1-MeV neutron energies.
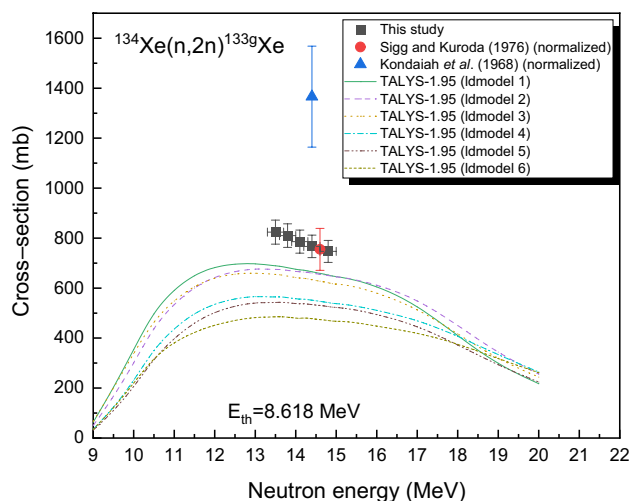
5.2 ^{134}Xe(n,2n)^{133g}Xe reaction

A thorough literature review yielded only one measurement of the ^{134}Xe(n,2n)^{133g}Xe reaction using γ-ray energy of 81 keV ($I_\gamma = 35\%$) [12]. However, many investigations have used $I_\gamma = 36.9\%$ for gamma rays with the same energy. Production of the ^{133g}Xe nucleus resulted in two characteristic gamma rays with similar energies, 79.61 keV
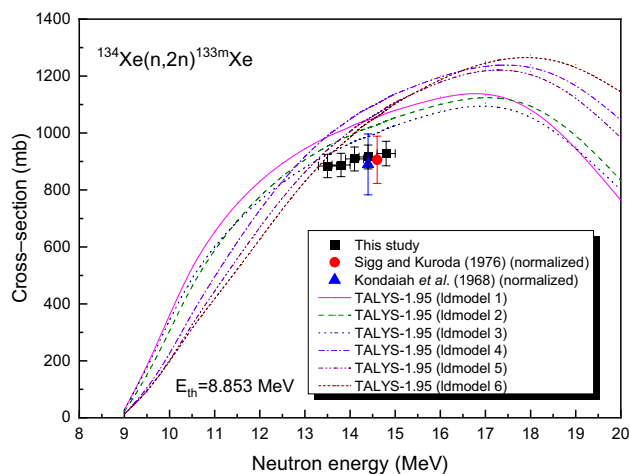
Fig. 3 (Color online) $^{134}Xe(n,2n)^{133m}Xe$ reaction CSs

($I_\gamma \square = 0.44\%$) and 80.998 keV ($I_\gamma \square = 36.9\%$). Our detectors could not resolve these energies; the intensity should be equal to their sum (37.34%). Accordingly, Eq. (8) was used to modify the CS values from Ref. [12]. During the $^{133\,m,g}Xe$ decay, the emitted 80.998-keV γ-ray was used to calculate the $^{134}Xe(n,2n)^{133g}Xe$ reaction CSs after subtracting the contribution of the $^{134}Xe(n,2n)^{133m}Xe$ reaction via the isomeric transition (IT). Almost 50% of the 80.998-keV γ-ray counts were from the isomeric transitions. Figure 4 shows the theoretical assessments of the excitation functions and the experimental results (Ref. [13] does not provide ground-state CS values, which are equal to the total CS value minus the excited-state CS value.). The measured values exceeded those calculated using the TALYS-1.95 software with ldmodels 1–6. However, our experimental and theoretical results show the same dependence on neutron energy.

At 14.6 MeV, our measurements agreed with the corrected values obtained by Sigg and Kuroda [12]. At 14.4 MeV, the results in Ref. [13] significantly exceeded our experimental and simulated results (using TALYS-1.95, ldmodels 1–6). For this reaction, the CS values span a wide energy range.
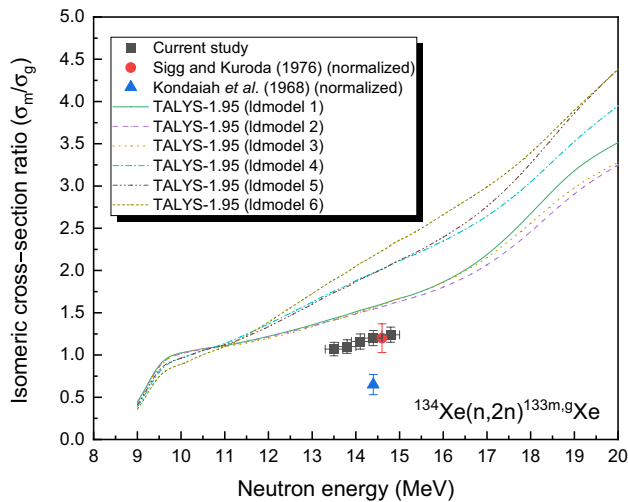
5.3 $^{134}Xe(n,2n)^{133}Xe$ reaction

There are two published reports on the $^{134}Xe(n,2n)^{133}Xe$ reaction at a neutron energy of 14 MeV that can be used to validate theoretical calculations and experimental results. The shapes of the excitation curves obtained from the ENDF/B-VIII.0 [35], (JEFF-3.3 [36], CENDL-3 [39]), JENDL-4.0 [37], and ROSFOND [38] databases were almost identical to those obtained by TALYS-1.95 [22] at ~ 15 MeV (Fig. 5). We conclude that the experimental data agree with the ROSFOND [38] results, TALYS-1.95 with ldmodel 1, and the corrected experimental results of Sigg and Kuroda [12]. At 14.4 MeV, the values [13] were 570 mb higher than ours. The evaluation excitation curve taken from JENDL-4.0 [37] is above the corrected results of Sigg and Kuroda [12], our experimental results, and results from the other databases [35, 36, 38, 39]. Data for the 13.5–14.1 MeV neutron energy range are reported for the first time.

5.4 Isomeric CS ratio

The ratios of the isomeric CSs were calculated using the measured $^{134}Xe(n,2n)^{133m,g}Xe$ CSs. The CS ratios (σ_m/σ_g) for the isomeric $^{133m,g}Xe$ pair created from the $^{134}Xe(n,2n)$ reaction exposed to incident neutrons with energies of 13.5 ± 0.2 MeV, 13.8 ± 0.2 MeV, 14.1 ± 0.2 MeV, 14.4 ± 0.2 MeV, and 14.8 ± 0.2 MeV are 1.07 ± 0.08, 1.10 ± 0.08, 1.16 ± 0.09, 1.20 ± 0.09, and 1.24 ± 0.09, respectively (Table 9). Figure 6 shows the corrected isomeric

Fig. 4 (Color online) $^{134}Xe(n,2n)^{133g}Xe$ reaction CSs
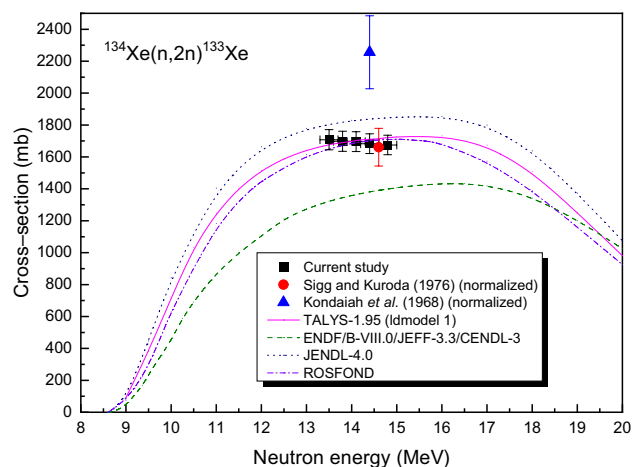
Fig. 5 (Color online) $^{134}Xe(n,2n)^{133}Xe$ reaction CSs

Fig. 6 (Color online) IRs of ^{134}Xe(n,2n)^{133m,g}Xe reactions as a function of neutron energy

CS ratios from the literature [12, 13] and the excitation curves obtained using TALYS-1.95 calculations for different density-level models. The isomeric CS ratios increased with energy. In the 14-MeV region, the isomeric CS ratio is directly correlated with the neutron energy, indicating that higher excitation energies result in high-spin isomers ($11/2^- \rightarrow 3/2^+$) [40–43]. The obtained σ_m/σ_g values were consistent with the modified values from Sigg and Kuroda [12], but slightly lower than the values obtained using ldmodels 1–6 and higher than the results of Ref. [13]. Our data for neutrons with 13.5–14.1 MeV energies are the first available in the literature to the best of our knowledge.

6 Summary and Conclusion

The σ_m, σ_g, and σ_{m+g} for the ^{134}Xe(n,2n)^{133m}Xe, ^{134}Xe(n,2n)^{133g}Xe, and ^{134}Xe(n,2n)^{133}Xe reactions and the corresponding isomeric CS ratios (σ_m/σ_g) were determined from the neutron activation and offline γ-ray spectra of the residual products at 13.5–14.8 MeV using the ^{93}Nb(n,2n)^{92m}Nb reaction as a reference. We thoroughly analyzed the uncertainties of the experimentally obtained CSs using covariance analysis. Experimental data were compared to data from the literature and CS values obtained using TALYS-1.95 software and from the ENDF/B-VIII.0, JEFF-3.3, JENDL-4.0, ROSFOND, and CENDL-3 databases. The theoretically obtained CS values for the ^{134}Xe(n,2n) reaction at six different NLDs (to generate nuclear excited and ground states) disagreed with the experimental results. However, the total CSs values were in agreement. The magnitude of the calculated CSs differed due to variations in the nuclear inputs and reaction models used for the simulations.

The reaction mechanism involves photon and particle emissions in the CN. The CN CS is determined by the OPs, NLDs, and γ SFs. Significant discrepancies were found in the experimental values; however, these were observed only for the pure ground state and total CSs as they are the most affected by the excited states. The CSs at neutron energies of 13.5–14.1 MeV are presented for the first time for the ^{134}Xe(n,2n)^{133m}Xe, ^{134}Xe(n,2n)^{133g}Xe, and ^{134}Xe(n,2n)^{133}Xe reactions, significantly extending the currently published energy ranges. These values can benefit nuclear databases for exploring fundamental nuclear applications and nuclear reaction models.

Author contributions All authors contributed to the study conception and design. Material preparation, data collection and analysis were performed by Jun-Hua Luo, Jun-Cheng Liang, Li Jiang, Fei Tuo, Liang Zhou, and Long He. The first draft of the manuscript was written by Jun-Hua Luo and all authors commented on previous versions of the manuscript. All authors read and approved the final manuscript.

References

1. X. Li, L. Liu, W. Jiang et al., Measurements of the ^{107}Ag neutron capture cross sections with pulse height weighting technique at the CSNS Back-n facility. Chin. Phys. B **31**, 038204 (2022). https://doi.org/10.1088/1674-1056/ac48fd

2. X. Hu, G. Fan, W. Jiang et al., Measurements of the ^{197}Au(n, γ) cross section up to 100 keV at the CSNS Back-n facility. Nucl. Sci. Tech. **32**, 101 (2021). https://doi.org/10.1007/s41365-021-00931-w

3. X. Hu, L. Liu, W. Jiang et al., New experimental measurement of natSe(n, γ) cross section between 1 eV to 1 keV at the CSNS Back-n facility. Chin. Phys. B **31**, 080101 (2022). https://doi.org/10.1088/1674-1056/ac6ee2

4. B. Jiang, J. Han, J. Ren et al., Measurement of 232Th(n, γ) cross section at the CSNS Back-n facility in the unresolved resonance region from 4 keV to 100 keV. Chin. Phys. B **31**, 060101 (2022). https://doi.org/10.1088/1674-1056/ac5394

5. J. Tang, Q. An, J. Bai et al., Back-n white neutron source at CSNS and its applications. Nucl. Sci. Tech. **32**, 11 (2021). https://doi.org/10.1007/s41365-021-00846-6

6. CINDA-A, The index to literature and computer files on microscopic neutron data, International Atomic Energy Agency, 2000.

7. V. Mclane, C.L. Dunford, P.F. Rose, *Neutron cross sections*, vol. 2 (Academic, New York, 1988)

8. F. Najmabadi, Prospects for attractive fusion power systems. Philos. Trans. Royal Soc. A **357**, 625–638 (1999). https://doi.org/10.1098/rsta.1999.0344

9. Evaluated Nuclear Structure Data File (ENSDF), (Last updated 2022–06–16) http://www.nndc.bnl.gov/ensdf/

10. A. Gandhi, A. Sharma, Y.N. Kopatch et al., Cross section calculation of (n, p) and (n,2n) nuclear reactions on Zn, Mo and Pb

isotopes with~14 MeV neutrons. J. Radioanal. Nucl. Chem. **322**, 89–97 (2019). https://doi.org/10.1007/s10967-019-06533-6

11. J. Luo, L. Jiang, Cross sections for (n,2n), (n, α), (n, p), (n, d) and (n, t) reactions on molybdenum isotopes in the neutron energy range of 13 to 15 MeV. Chin. Phys. C **44**, 114002 (2020). https://doi.org/10.1088/1674-1137/abaded

12. R.A. Sigg, P.K. Kuroda, 146-MeV neutron activation cross section for the xenon isotopes. Nucl. Sci. Eng. **60**, 235–238 (1976). https://doi.org/10.13182/NSE76-A26880

13. E. Kondaiah, N. Ranakumar, R.W. Fink, Thermal neutron activation cross sections for Kr and Xe isotopes. Nucl. Phys. A **120**, 329–336 (1968). https://doi.org/10.1016/0375-9474(68)90769-0

14. C. Bhatia, S.W. Finch, M.E. Gooden et al., ^{136}Xe(n,2n)^{135}Xe cross section between 9 and 15 MeV. Phys. Rev. C **87**, 011601(R) (2013). https://doi.org/10.1103/PhysRevC.87.011601

15. M. Bhike, W. Tornow, Neutron-capture cross-section measurements of 136Xe between 0.4 and 14.8 MeV. Phys. Rev. C **89**, 031602(R) (2014). https://doi.org/10.1103/PhysRevC.89.031602

16. B. Megha Bhike, M.E. FallinGooden et al., Comprehensive sets of ^{124}Xe(n, γ)^{125}Xe and ^{124}Xe(n,2n)^{123}Xe cross-section data for assessment of inertial-confinement deuterium-tritium fusion plasma. Phys. Rev. C **91**, 011601(R) (2015). https://doi.org/10.1103/PhysRevC.91.011601

17. J. Luo, L. Jiang, J. Liang et al., Cross-section measurements of the (n,2n) and (n, p) reactions on ^{124,126,128,130,131,132}Xe in the 14 MeV region and theoretical calculations of their excitation functions. Chin. Phys. C **46**, 044001 (2022). https://doi.org/10.1088/1674-1137/ac3fa4

18. J. Luo, J. Liang, L. Jiang et al., Cross-sections and isomeric ratios for the ^{136}Xe(n,2n)$^{135m, g}$Xe reactions in the 14 MeV region with covariance analysis. Eur. Phys. A **58**, 142 (2022). https://doi.org/10.1140/epja/s10050-022-00797-5

19. J. Luo, L. Jiang, L. Shan et al., Determination of the cross-section for (n, p) and (n, α) reactions on ^{153}Eu at neutron energies from 13 to 15 MeV. J. Phys. G Nucle. Part. Phys. **47**, 075104 (2020). https://doi.org/10.1088/1361-6471/ab8d8f

20. Q. Wang, B. Chen, Q. Zhang et al., Cross-section measurement of (n,2n) reactions for Nd isotopes induced by 14 MeV neutrons. Nucl. Sci. Tech. **30**, 8 (2019). https://doi.org/10.1007/s41365-018-0535-5

21. Y. Song, F. Zhou, Y. Li et al., Methods for obtaining characteristic γ-ray net peak count from interlaced overlap peak in HPGe γ-ray spectrometer system. Nucl. Sci. Tech. **30**, 11 (2019). https://doi.org/10.1007/s41365-018-0525-7

22. A. Koning, S. Hilaire and M. Duijvestijn, TALYS-1.95, A nuclear reaction program, NRG-1755 ZG Petten, The Netherlands, 2019, http://www.talys.eu

23. International Reactor Dosimetry and Fusion File, IRDFF-II, January, 2020 https://www-nds.iaea.org/IRDFF/

24. J. Luo, L. Du, J. Zhao, A method to determine fast neutron energies in large sample. Nucl. Instrum. Meth. B **298**, 61–65 (2013). https://doi.org/10.1016/j.nimb.2013.01.029

25. V.E. Levis, K.J. Zieba, A transfer standard for d+T neutron fluence and energy. Nucl. Instrum. Methods **174**, 141–144 (1980). https://doi.org/10.1016/0029-554X(80)90422-X

26. GammaVision®-32, Gamma-ray spectrum analysis and MCA emulator, software user's manual, software version 5.3

27. N. Otuka, B. Lalremruata, M.U. Khandaker et al., Uncertainty propagation in activation cross section measurements. Rad. Phys. Chem. **140**, 502–510 (2017). https://doi.org/10.1016/j.radphyschem.2017.01.013

28. A. Gandhi, A. Sharma, R. Pachauri et al., Neutron capture reaction cross section measurement for iodine nucleus with detailed uncertainty quantification. Eur. Phys. J. Plus **136**, 819 (2021). https://doi.org/10.1140/epjp/s13360-021-01824-y

29. A. Gandhi, A. Sharma, R. Pachauri et al., Measurement of (n, α) and (n,2n) reaction cross sections at a neutron energy of 14.92 ± 0.02 MeV for potassium and copper with uncertainty propagation. Chin. Phys. C **46**, 014002 (2022). https://doi.org/10.1088/1674-1137/ac2ed4

30. A. Gandhi, A. Sharma, A. Kumar et al., Measurement of (n, γ), (n, p), and (n,2n) reaction cross sections for sodium, potassium, copper, and iodine at neutron energy 14.92±0.02 MeV with covariance analysis. Phys. Rev. C **102**, 014603 (2020). https://doi.org/10.1103/PhysRevC.102.014603

31. W. Dilg, W. Schantl, H. Vonach et al., Level density parameters for the back-shifted fermi gas model in the mass range 40 < A < 250. Nucl. Phys. A **217**, 269–298 (1973). https://doi.org/10.1016/0375-9474(73)90196-6

32. A.V. Ignatyuk, J.L. Weil, S. Raman et al., Density of discrete levels in ^{116}Sn. Phys. Rev. C **47**, 1504–1513 (1993). https://doi.org/10.1103/PhysRevC.47.1504

33. R. Capote, M. Herman, P. Obložinský et al., RIPL–reference input parameter library for calculation of nuclear reactions and nuclear data evaluations. Nucl. Data Sheets **110**, 3107–3214 (2009). https://doi.org/10.1016/j.nds.2009.10.004

34. R.K. Singh, N.L. Singh, R.D. Chauhan et al., Systematic study of the (n, 2n) reaction cross section for ^{121}Sb and ^{123}Sb isotopes. Chin. Phys. C **46**, 054002 (2022). https://doi.org/10.1088/1674-1137/ac4a5a

35. ENDF/B-VIII.0 (USA, 2018), Evaluated Nuclear Data File (ENDF) Database Version of 2021–06–28

36. JEFF-3.3 (Europe, 2017), Evaluated Nuclear Data File (ENDF) Database Version of 2022–04–22

37. JENDL-4.0 (Japan,2012), Evaluated Nuclear Data File (ENDF) Database Version of 2022–04–22

38. ROSFOND (Russia, 2010), Evaluated Nuclear Data File (ENDF) Database Version of 2022–04–22 https://www-nds.iaea.org/exfor/endf.htm

39. CENDL-3 (China, 2020), Evaluated Nuclear Data File (ENDF) Database Version of 2022–04–22

40. S.M. Qaim, A. Mushtaq, M. Uhl, Isomeric cross-section ratio for the formation of $^{73m, g}$Se in various nuclear processes. Phys. Rev. C **38**, 645–650 (1988). https://doi.org/10.1103/PhysRevC.38.645

41. S.M. Qaim, M. Ibn. Majah, R. Wölfle et al., Excitation functions and isomeric cross-section ratios for the ^{90}Zr(n,p)^{90}Y^{m,g} and ^{91}Zr(n,p)^{91}Y^{m,g} processes. Phys. Rev. C **42**, 363–367 (1990). https://doi.org/10.1103/PhysRevC.42.363

42. C.D. Nesaraja, S. Sudár and S.M. Qaim, Cross sections for the formation of ^{69}Zn^{m,g} and ^{71}Zn^{m,g} in neutron induced reactions near their thresholds: Effect of reaction channel on the isomeric cross-section ratio. Phys. Rev. C **68**, 024603 (2003). https://doi.org/10.1103/PhysRevC.68.024603

43. S.M. Qaim, Total (n, 2n) cross sections and isomeric cross-section ratios at 14.7 MeV in the region of rare earths. Nucl. Phys. A **224**, 319–330 (1974). https://doi.org/10.1016/0375-9474(74)90690-3